Light-Emitting Halide Perovskite Nanoantennas

Journal:	*Nano Letters*
Manuscript ID	nl-2017-04727h.R1
Manuscript Type:	Communication
Date Submitted by the Author:	n/a
Complete List of Authors:	Tiguntseva, Ekaterina; Sankt Peterburgskij nacional'nyj issledovatel'skij universitet informacionnyh tehnologij mehaniki i optiki Zograf, George; ITMO University, Nanophotonics and Metamaterials Komissarenko, Filipp; St Petersburg Academic University Zuev, Dmitry; ITMO University, Zakhidov, Anvar; The University of Texas, Makarov, Sergey; ITMO University, The Metamaterials Laboratory Kivshar, Yuri; Australian National University, Nonlinear Physics Center

Light-Emitting Halide Perovskite Nanoantennas

E.Y. Tiguntseva,[†] G.P. Zograf,[†] F.E. Komissarenko,[†] D.A. Zuev,[†]

A.A. Zakhidov,[†,‡] S.V. Makarov,[*,†] and Yu.S. Kivshar[*,†,¶]

[†]*Department of Nanophotonics and Metamaterials, ITMO University, St. Petersburg, 197101, Russia*

[‡]*University of Texas at Dallas, Richardson TX 75080, United States*

[¶]*Nonlinear Physics Centre, Australian National University, Canberra ACT 2601, Australia*

E-mail: s.makarov@metalab.ifmo.ru; yuri.kivshar@anu.edu.au

Abstract

Nanoantennas made of high-index dielectrics with low losses in visible and infrared frequency ranges have emerged as a novel platform for advanced nanophotonic devices. On the other hand, halide perovskites are known to possess high refractive index, and they support excitons at room temperature with high binding energies and quantum yield of luminescence that makes them very attractive for all-dielectric resonant nanophotonics. Here we employ halide perovskites to create *light-emitting nanoantennas* with enhanced photoluminescence due to the coupling of their excitons to dipolar and multipolar Mie resonances. We demonstrate that the halide perovskite nanoantennas can emit light in the range of 530–770 nm depending on their composition. We employ a simple technique based on laser ablation of thin films prepared by wet-chemistry methods as a novel cost-effective approach for the fabrication of resonant perovskite nanostructures.

Keywords

Halide perovskites, photoluminescence, nanoantenna, Mie resonance, Purcell effect

Subwavelength sources of visible photons are basic elements for advanced nanophotonic circuits[1]. Single molecules[2], quantum dots[3] and nanoparticles with active defects[4] are the most frequently used light emitters. The main challenges are to optimize emitters efficiency[5], couple effectively their emission to free space or steer radiation pattern to a given direction[3,6]. In order to achieve these goals, various designs of nanoantennas have been suggested, where the emitters are placed near them. Both plasmonic[7,8] and all-dielectric[9,10] nanoantennas exhibit strong incident light localization and high values of the Purcell factor. However, low-loss all-dielectric nanoantennas[11] allow placing light sources inside a bulk material[12,13], protecting them from harmful ambient conditions such as chemical pollution or mechanical damages.

Another approach is to create light-emitting dielectric nanoantennas with optical resonances at the wavelength of the material emission. For example, such materials as GaAs and GaN possess direct interband transitions with light emission, while their refractive indices are high enough to support strong Mie resonances in the visible range. Resonant nanostructures with low defect concentration and low losses could be employed as effective nanoscale light sources. However, the costs of multistage fabrication of nanostructures (placed on low-index substrates for high optical contrast) made of active inorganic semiconductors is a limiting factor for their practical implementation.

On the other hand, organic-inorganic (hybrid) perovskites of the $MAPbX_3$ family, where methylammonium (MA) stands for CH_3NH_3, and X stands for I, Br or Cl, represent a class of dielectric materials with excitonic states at room temperature, refractive indices (n=2–3) high enough for the efficient excitation of Mie resonances, low losses at the exciton wavelength, chemically tunable band gap[14], high defect tolerance[15], and high quantum yield (more than 30%[16]) of photoluminescence. These properties make them perfect candidates for effective nanoscale light sources. Superior properties, along with low fabrication cost (wet-

chemistry or chemical-vapor deposition), allow for creating hybrid perovskite light-emitting metasurfaces[17,18] and microparticles[19]. Additionally, the emitting wavelengths of hybrid perovskites can be gradually tuned over the entire visible range (400–800 nm) by simple replacing or mixing the anion compound (I, Br or Cl)[20].

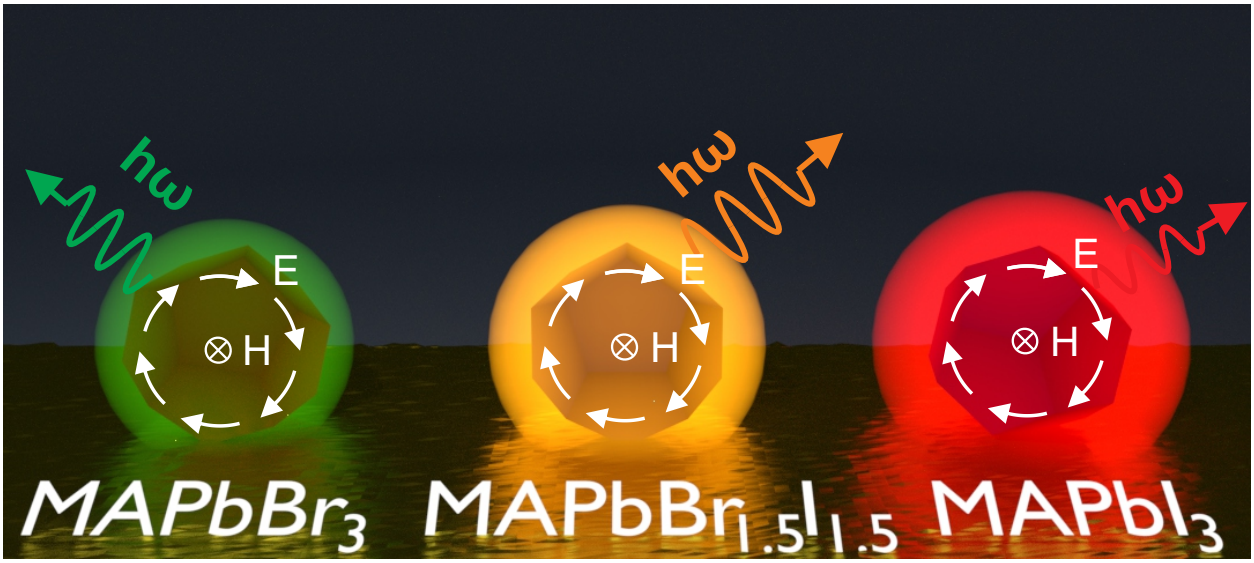

Figure 1: **Schematic of tunable light-emitting halide perovskite nanoantennas**. Left to right: a nanoparticle emits light at different wavelengths depending on its chemical structure.

Here we suggest and fabricate perovskite nanoparticles supporting electric and magnetic dipolar and multipolar Mie resonances. When the light emission occurs at the resonant conditions, we observe five-fold enhancement of normalized-to-volume photoluminescence (PL) for resonant nanoparticles and up to two-fold enhancemnet as compared with a thin perovskite film due to the Purcell effect. Simplicity of perovskite nanoparticle fabrication allows for changing the PL line position (from red to greed) by varying the anion (I and Br), as shown schematically in Fig 1. We believe this is the first demonstration of halide perovskite subwavelength nanoantennas with the spectrally variable emission enhanced by Mie resonances.

Fabrication of $MAPbI_3$ nanoparticles. For fabrication of nanoparticles, we employ the laser printing method[21]. In this approach, nanoparticles are fabricated from a perovskite

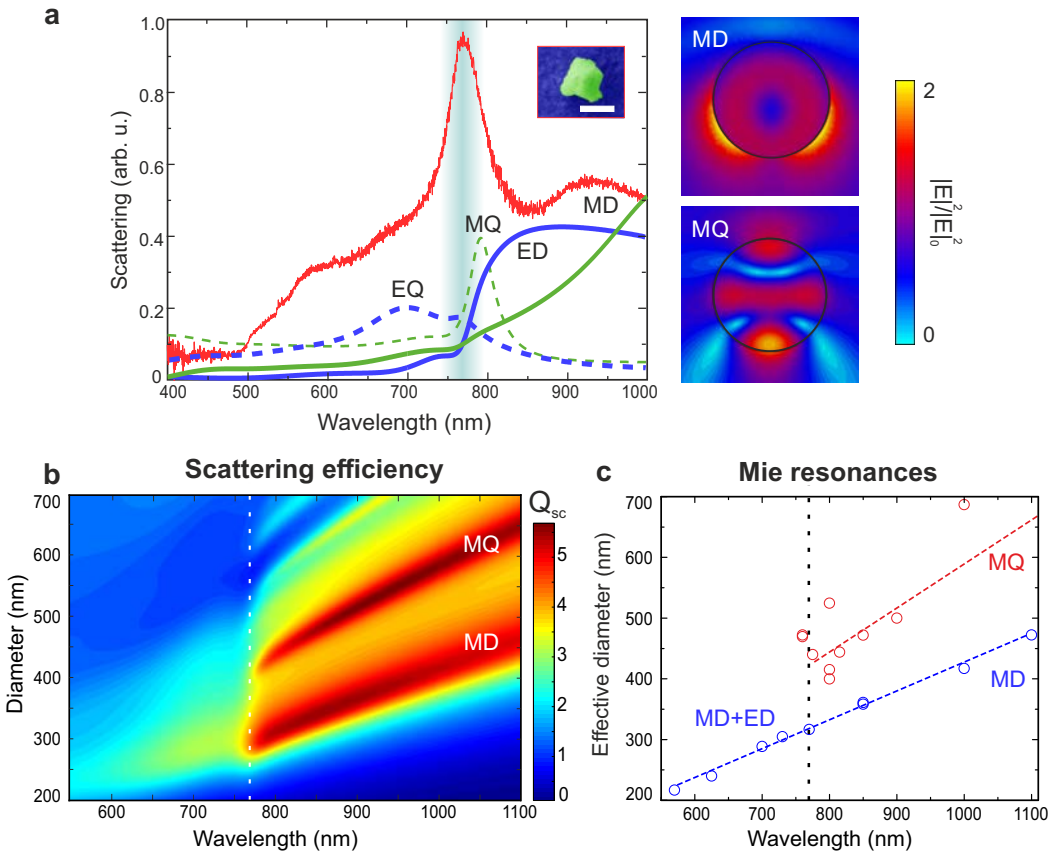

Figure 2: **Resonant properties of $MAPbI_3$ perovskite nanoparticles**. (a) Red curve corresponds to experimental dark-field scattering spectrum for single perovskite nanoparticle with diameter 415 nm. Lines stand for analytical mode decomposition for single spherical perovskite nanoparticle of 440 nm in homogeneous air media (green dashed line - magnetic quadrupole (MQ), green solid line - magnetic dipole (MD), blue dashed line - electric quadrupole (EQ), blue solid line- electric dipole (ED)). Right: Electric field distributions at wavelength 790 nm and 1000 nm for the perovskite nanoparticle. (b) Calculated map of scattering efficiency (Q_{sc}) for a spherical perovskite nanoparticle in air (Mie theory), showing dependencies on the particle diameter and incident wavelength. (c) Experimental (dots) and theoretical (dash lines) values of resonances spectral positions depending on the diameter of perovskite nanoparticles. Red and blue colors corresponds to the position of magnetic quadrupole (MQ) and magnetic dipole (MD) resonances respectively.

thin film in the forward-transfer geometry, when the receiving substrate is placed under the film with a spacing of 50 μm. For a film, solution of perovskite precursor ($MAPbI_3$) is prepared in a dry-box as follows: methylammonium iodide (MAI) in γ-butyrolactone with dimethyl sulfoxide (GBL:DMSO) at the concentration of 1.5 M is used to dissolve 1.5M of lead iodine (PbI_2). The solution is stirred and heated (70°C) overnight and used after filtration through 0.45 μm PTFE syringe filter. For depositing, a perovskite layer is created by a solvent-engineering technique inside the dry-box, including two step spin-coating process[22]. At the first step, a solution precursor $MAPbI_3$ is deposited at rotation speed 1000 rpm. The second step is the dripping 200 μl of the toluene at 3000 rpm, which does not dissolve perovskite during the film formation. Each film is annealed at 100°C for 10 min[22]. Glass substrates are washed by sonication in dianized water, toluene, acetone, and isopropanol, consequently. Despite low cost and simplicity, this method allows for the formation of high-quality films emitting light with high quantum yield (up to 70 %)[23]. The perovskite nanoparticles are fabricated by employing Yb^{+3} femtosecond laser pulses at $\lambda = 1050\ nm$ with energy around 50 nJ focused by 10× objective (NA=0.25). Morphology and size of the nanoparticles are studied by scanning electron microscopy (SEM) with an electron microscope (Crossbeam 1540 XB, Carl Zeiss). According to our data, the size of nanoparticles is in the range of 50–500 nm, their shape is quasi-spherical with some facets, whereas their position on a receiving substrate is random (for details, see *Supporting information*).

Optical properties of nanoparticles. First, we study optical resonances of the fabricated perovskite nanoparticles deposited on a silica glass substrate, by using confocal dark-field optical spectroscopy. In our experiments, the nanoparticles are excited at an oblique angle (65 degrees with respect to the normal of the surface) by linearly polarized light from a halogen lamp (HL-2000-FHSA) through a weakly-focusing objective (Mitutoyo M Plan Apo NIR, 10×, NA=0.28). Scattered light is collected from the top by an 50× objective (Mitutoyo M Plan APO NIR, NA=0.42), sent to Horiba LabRam HR spectrometer and pro-

jected onto a thermoelectrically cooled charge-coupled device (CCD, Andor DU 420A-OE 325) with a 150-g/mm diffraction grating.

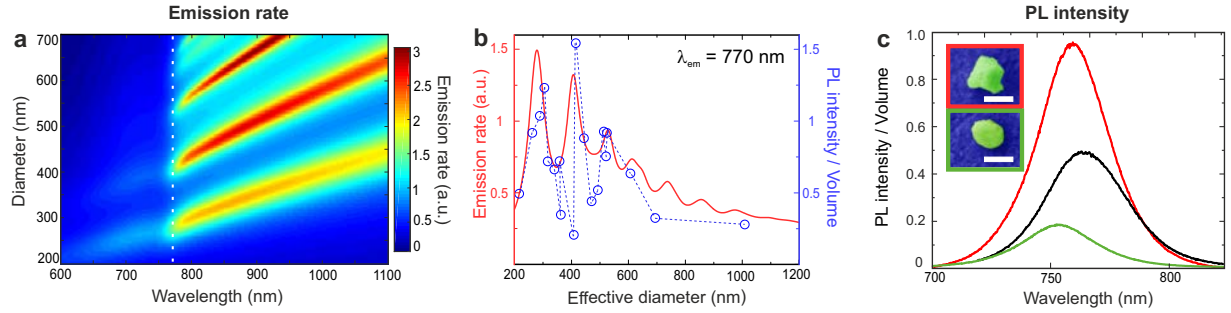

Figure 3: **PL enhancement from $MAPbI_3$ resonant nanoparticles**. (a) Calculated emission rate for spherical perovskite nanoparticles in air. Dash white line marks the position of the exciton line around 770 nm. (b) Comparison of experimental data (dots) of photoluminescence normalized to nanoparticle's volume with theoretical results (line) for the emission rate of a dipole placed inside the spherical perovskite nanoparticle. (c) Photoluminescence spectra normalized to the volume for perovskite nanoparticles of different sizes shown in the inset with the SEM images and marked by the corresponding colors of the frames, as well as for 0.5 μm perovskite film. Scale bar in the SEM images is 400 nm.

The study of white-light scattering from the perovskite nanoparticles with different diameters reveals their resonant behavior in both visible and infrared ranges. For example, as shown in Fig. 2a, a nanoparticle with diameter 415 nm (measured by SEM) exhibits a pronounced maximum around the spectral position of the exciton line ($\lambda \approx 770$ nm). According to our analytical calculations based on the mode decomposition with the Mie theory (for details, see *Supporting Information*), the experimentally obtained spectrum can be theoretically described by several Mie resonant modes in 440 nm spherical perovskite nanoparticle. Namely, magnetic dipole (MD), electric dipole (ED), magnetic quadrupole (MQ), and electric quadrupole (EQ) modes contribute to the dark-field spectra in the low-loss range (i.e. $\lambda > 750$ nm). As shown in the inset to Fig. 2a and *Supporting Information*, a spherical shape of nanoparticles is a reasonable approximation for our modeling, in agreement with previous studies of dielectric nanoparticles with facets[24,25]. Also, the spectral positions of the Mie resonances are not affected significantly by a substrate[26] or angle of incidence (see *Supporting Information*). Full-wave numerical simulations with CST Microwave Studio for perovskite

nanospheres with the same diameter allows for visualization of near-field structure at MD and MQ resonances, which is typical for high-index dielectric nanoparticles. Computational domain is chosen to be $2 \times 2 \times 2\ \mu m^3$. Optical properties of $MAPbI_3$ perovskite are taken from the literature[27].

As shown in Fig. 2b, theoretical results for light scattering by a $MAPbI_3$ sphere reveal a variation of the Mie resonances in a broad range of nanoparticles' diameters (200–700 nm). All resonances demonstrate a red shift with an increase of the nanoparticle diameter, in agreement with previous studies[11]. By measuring the dark-field spectra from perovskite nanoparticles of different sizes, we find the same dependences for distinguishable MD and MQ modes, as shown in Fig. 2c. Importantly, although electric and magnetic modes are quite distinguishable in the low-loss spectral range, they are strongly overlapped at the wavelengths shorter than that corresponding to the conduction band edge, as shown in Fig. 2c and discussed in *Supporting Information*.

$MAPbI_3$ nanoparticles as light-emitting nanoantennas. According to the previous studies, we expect that perovskite nanoparticles should enhance the rate of spontaneous emission via the Purcell effect, thus increasing the quantum yield and PL intensity[28,29]. Figure 3a shows the calculated enhancement of the emission rate (emitted power) for a point dipole in a perovskite sphere, normalized to the corresponding values for the dipole in vacuum. We consider different diameters (200–700 nm) and wavelengths (λ=600–1100 nm), and average the calculated values of the emitted power over nanoparticle's volume and orientations of the dipole. A theoretical approach that we use is based on an early developed model[30] (for details, see *Supporting information*). Optical properties of $MAPbI_3$ perovskite are taken from the literature[27].

As observed in our experiments on laser photoexcitation of perovskite nanoparticles, the optical Mie resonances affect the intensity of PL emission (see Fig. 3b). In particular, when the spectral position of the exciton line coincides with the position of the MQ resonance, the PL signal normalized to the emitting material volume becomes more than five times

stronger than that for slightly smaller nanoparticles and two times stronger in comparison with 0.5 μm perovskite film, as shown in Fig. 3c. It is clearly seen that the PL enhancement via the Purcell effect is possible due to the resonant behavior at the exciton wavelength in hybrid perovskites $MAPbI_3$ (770 nm at room temperature). Matching the peaks in the experimental dark-field spectra from various perovskite nanoparticles with those obtained theoretically allows to define the effective diameters for various perovskite nanoparticles with slightly non-spherical shapes (see insets in Fig. 3c). Finally, we plot the experimental dependence of the PL signal normalized to the nanoparticle's volume on their diameter (see Fig. 3b). Experimental values of the PL enhancement show a nonmonotonic dependence correlating with the theoretical dependence of the enhanced emission rate on the size of nanoparticles. Some discrepancy can be assciated to a neglected substrate and facets in the analytical calculations of the emission rate.

The PL measurements are carried out by using the same setup as for dark-field measurements, by exciting nanoparticles by light of λ=530 nm with spectral width 10 nm generated from filtered supercontinuum (repetition rate 80 MHz, pulse duration 7 ps, model Fianium SC 400) with average power 10 mW. The volume of nanoparticles for the PL normalization is calculated as that of an effective sphere with a known radius, whereas the volume for photoexcited region is calculated as that of an elliptic rod with the height equal to the film thickness and radii derived from the size of the incident beam. Some blue spectral shift of the nanoparticles PL relative to the film spectrum was reported previously for $MAPbI_3$ nanoparticles of sub-100-nm sizes[31].

Perovskite nanoantennas with mixed anions for variation of emission spectrum. Tunability of nanoantennas is highly desired for many applications related to nanophotonic devices[32]. Energy band structure and emission properties of all-dielectric nanostructures can be changed by only using different materials (such as Si[33], AlGaAs[34], GaP[29]) or doping[35]. However, changing the material in the current semiconductor technologies leads to additional requirements to entire fabrication process (deposition and etching), while the

ion doping can not gradually tune emission line over hundreds nanometers.

In turn, methylammonium lead trihalide perovskites have been the most intensively explored so far in optoelectronics, and they can possess a composition with mixed anions X and Y, i.e. $MAPbX_nY_{3-n}$, resulting in gradual tuning of PL emission line[20]. Following the simple protocol[36–38], we create $MAPbBr_3$ and $MAPbBr_{1.5}I_{1.5}$ thin films and fabricate nanoparticles by the same method as described before for $MAPbI_3$. In Fig. 4 we present PL and scattering spectra of nanoparticles with different compositions, exhibiting a broad range of spectral tuning: from $\lambda\approx$770 nm, for $MAPbI_3$, down to $\lambda\approx$530 nm, for $MAPbBr_3$, though intermediate state $\lambda\approx$660 nm for $MAPbBr_{1.5}I_{1.5}$. Importantly, to avoid unstable behavior of PL from the mixed halide composition ($MAPbBr_{1.5}I_{1.5}$) due to segregation effect[14,39], we apply illumination with average pump intensities around 0.1 W/cm^2.

According to the Moss law[40], for all semiconductors real part of the refractive index n decreases with an increase of the band gap E_g in accord with the formula $n^4 \approx const/E_g$, meaning that n should decrease slightly after a change of the perovskite halide composition from I to Br anions. Namely, from the values n=2.4–2.6 for $MAPbI_3$ down to 1.8–2.3 for $MAPbBr_3$ (for details, see *Supporting information*). Moreover, imaginary part of the refractive index decreases over more than one order of magnitude in the spectral range 570–770 nm after replacing iodine by bromine. The shift of energy band structure and, thus, complex refractive index, is crucial for optical properties of the perovskite nanoparticles. In Figs. 4(a,c,e), the scattering spectra of nanoparticles with close diameters (≈250 nm) exhibit resonant behavior with strong contributions from MD and ED resonances, as confirmed by corresponding numerical modeling, see Figs. 4(b,d,f).

These results directly show a strong dependence of the spectral position of resonances on the composition of perovskites and their complex refractive index. In particular, the positon of the MD resonance shifts from 600 nm to 770 nm when bromine replaces iodine in the $MAPb(Br_nI_{1-n})_3$ composition. Remarkably, MD is weaker than ED in high-loss spectral ranges (frequencies are higher than those for excitons or PL), and vice versa for the low-

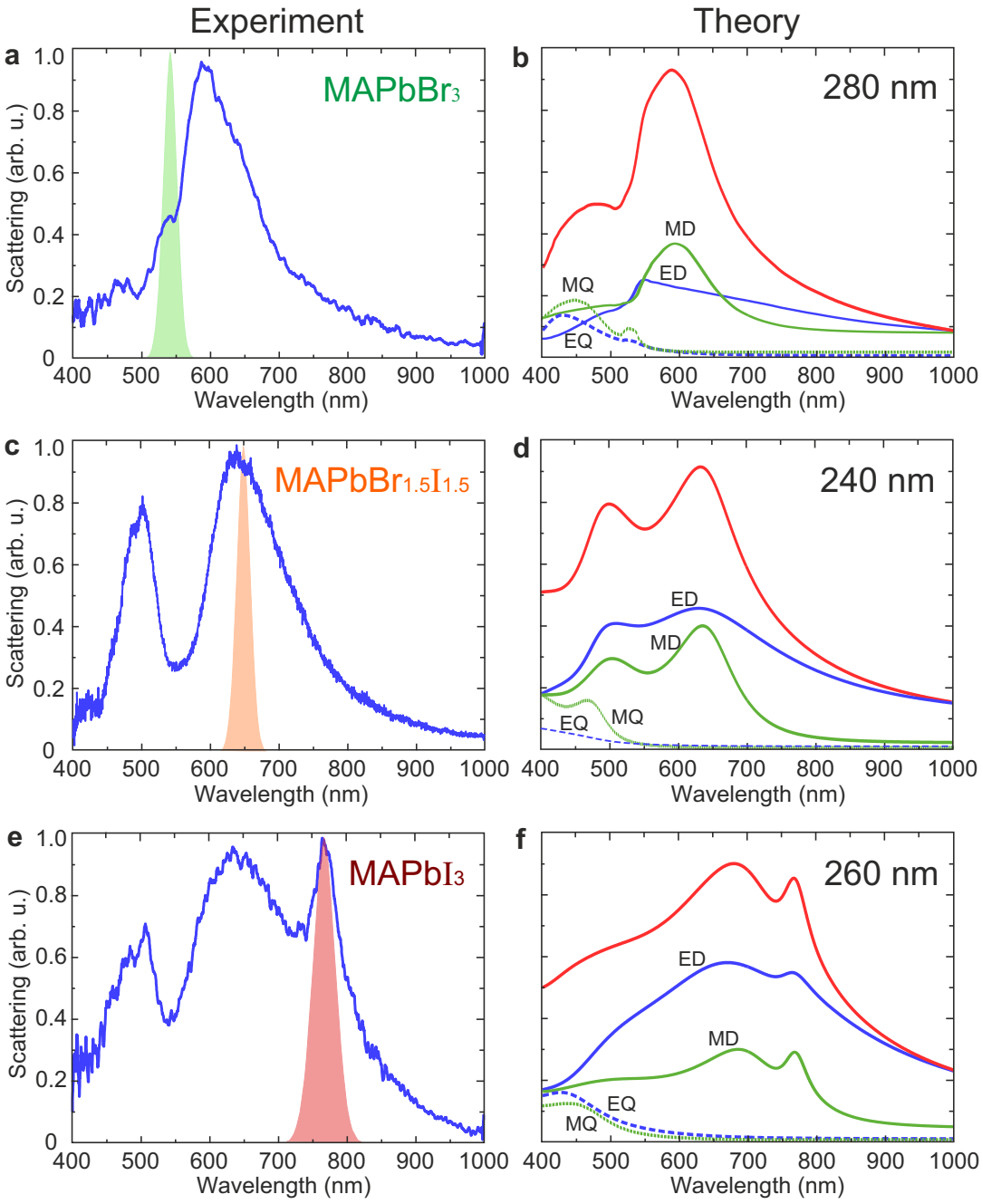

Figure 4: **Resonant properties of perovskite nanoparticles with different composition**. (a,c,e) Blue curve corresponds to experimental dark-field scattering spectra for single perovskite nanoparticles of different composition on a glass substrate. Filled color areas correspond to experimentally measured PL spectra of perovskite nanoparticles. (b,d,f) Red solid line shows analytical scattering spectrum in dark-field configuration for $MAPbBr_3$, $MAPbBr_{1.5}I_{1.5}$, $MAPbI_3$ perovskite nanoparticles with diameters of 280 nm, 240 nm, and 260 nm, respectively. Green and blue lines stand for the mode decomposition in air (green dashed – MQ, blue dashed – EQ, green solid – MD, blue solid – ED).

loss range, as shown in Figs. 4(b,d,f). Such a simple variation of the resonant properties via a change of one element (anion) in the chemical composition by using slightly different chemical protocols, simplifies the technological process for fabrication of light-emitting nanophotonic devices operating in a broad range of wavelengths. In this way, flexibility of band structure of the $MAPb(Br_nI_{1-n})_3$ perovskites[14] and high quantum yield (QY) at room temperature (more than 30%[16]) are superior to classical bulk semiconductors (e.g. resonant Si nanospheres[41] with QY<0.1%) and integrated nanoscale sources (Ge quantum dots within Si resonant nanodisks with QY≈1%[13,42] and Si nanocrystals within resonant SiO_2 nanodisks with QY<5%[12]) employed previously for all-dielectric nanoantennas.

Conclusion. We have proposed a novel type of light-emitting nanoantennas made of hybrid perovskites which demonstrate enhanced photoluminescence normalized to volume due to a coupling of excitons to Mie resonances. The observed enhancement is up to five-fold between various nanoparticles and up to two-fold as compared with a thin perovskite film. We have also demonstrated that optical properties of the perovskite nanoantennas can be changed in the range of 530-770 nm by a simple variation of their composition. Moreover, high defects tolerance of halide perovskites allows for creation of light-emitting nanoantennas even by the high throughput laser printing method involving strong heating and fast cooling of the target material. Our results pave the way towards new optoelectronics applications of nanophotonics based on halide perovskite materials.

Supporting Information

Supporting Information Available: Additional modeling and modeling details, more SEM images of the samples, details on laser printing.

Acknowledgements

The authors are indebted to R. Savelyev, E. Ushakova, M. Petrov, and R. Haroldsson for useful discussions, A. Ishteev for a help with sample preparation, and D. Permyakov for experimental setup acquisition. This work was supported by the Ministry of Education and Science of the Russian Federation (Project 14.Y26.31.0010 for optical measurements), Russian Science Foundation (Project 17-73-20336 for calculations), and the Australian Research Council. We also appreciate a partial support of the Welch Foundation grant AT 16-17.

References

(1) Tame, M. S.; McEnery, K.; Özdemir, Ş.; Lee, J.; Maier, S.; Kim, M. *Nature Physics* **2013**, *9*, 329–340.

(2) Kühn, S.; Håkanson, U.; Rogobete, L.; Sandoghdar, V. *Physical Review Letters* **2006**, *97*, 017402.

(3) Curto, A. G.; Volpe, G.; Taminiau, T. H.; Kreuzer, M. P.; Quidant, R.; van Hulst, N. F. *Science* **2010**, *329*, 930–933.

(4) Hausmann, B. J. M.; Shields, B. J.; Quan, Q.; Chu, Y.; de Leon, N. P.; Evans, R.; Burek, M. J.; Zibrov, A. S.; Markham, M.; Twitchen, D. *Nano Letters* **2013**, *13*, 5791–5796.

(5) Akselrod, G. M.; Argyropoulos, C.; Hoang, T. B.; Ciracì, C.; Fang, C.; Huang, J.; Smith, D. R.; Mikkelsen, M. H. *Nature Photonics* **2014**, *8*, 835–840.

(6) Lodahl, P.; Mahmoodian, S.; Stobbe, S. *Reviews of Modern Physics* **2015**, *87*, 347.

(7) Hoang, T. B.; Akselrod, G. M.; Argyropoulos, C.; Huang, J.; Smith, D. R.; Mikkelsen, M. H. *Nature Communications* **2015**, *6*, 1–7.

(8) Chikkaraddy, R.; de Nijs, B.; Benz, F.; Barrow, S. J.; Scherman, O. A.; Rosta, E.; Demetriadou, A.; Fox, P.; Hess, O.; Baumberg, J. J. *Nature* **2016**, *535*, 127–130.

(9) Bakker, R. M.; Permyakov, D.; Yu, Y. F.; Markovich, D.; Paniagua-Domínguez, R.; Gonzaga, L.; Samusev, A.; Kivshar, Y.; Lukyanchuk, B.; Kuznetsov, A. I. *Nano Letters* **2015**, *15*, 2137–2142.

(10) Krasnok, A.; Glybovski, S.; Petrov, M.; Makarov, S.; Savelev, R.; Belov, P.; Simovski, C.; Kivshar, Y. *Applied Physics Letters* **2016**, *108*, 211105.

(11) Kuznetsov, A. I.; Miroshnichenko, A. E.; Brongersma, M. L.; Kivshar, Y. S.; Lukyanchuk, B. *Science* **2016**, *354*, aag2472.

(12) Capretti, A.; Lesage, A.; Gregorkiewicz, T. *ACS Photonics* **2017**, *4*, 2187–2196.

(13) Rutckaia, V.; Heyroth, F.; Novikov, A.; Shaleev, M.; Petrov, M. I.; Schilling, J. *Nano Letters* **2017**, *17*, 6886–6892.

(14) Sutter-Fella, C. M.; Li, Y.; Amani, M.; Ager III, J. W.; Toma, F. M.; Yablonovitch, E.; Sharp, I. D.; Javey, A. *Nano Letters* **2015**, *16*, 800–806.

(15) Yin, W.-J.; Shi, T.; Yan, Y. *Applied Physics Letters* **2014**, *104*, 063903 .

(16) Koch, S.; Burke, S.; Paranji, R. K.; Shropshire, A. J.; Ziffer, M. E.; Ginger, D. S. *ACS Energy Lett.* **2016**, *1*, 438–444 .

(17) Makarov, S. V.; Milichko, V.; Ushakova, E. V.; Omelyanovich, M.; Cerdan Pasaran, A.; Haroldson, R.; Balachandran, B.; Wang, H.; Hu, W.; Kivshar, Y. S.; Zakhidov, A. A. *ACS Photonics* **2017**, *4*, 728–735.

(18) Gholipour, B.; Adamo, G.; Cortecchia, D.; Krishnamoorthy, H. N.; Birowosuto, M.; Zheludev, N. I.; Soci, C. *Advanced Materials* **2017**, *29*, 1604268.

(19) Tang, B.; Dong, H.; Sun, L.; Zheng, W.; Wang, Q.; Sun, F.; Jiang, X.; Pan, A.; Zhang, L. *ACS Nano* **2017**, *11*, 10681–10688.

(20) Sutherland, B. R.; Sargent, E. H. *Nature Photonics* **2016**, *10*, 295–302.

(21) Dmitriev, P.; Makarov, S.; Milichko, V.; Mukhin, I.; Gudovskikh, A.; Sitnikova, A.; Samusev, A.; Krasnok, A.; Belov, P. *Nanoscale* **2016**, *8*, 5043–5048.

(22) Jeon, N. J.; Noh, J. H.; Kim, Y. C.; Yang, W. S.; Ryu, S.; Seok, S. I. *Nature Materials* **2014**, *13*, 897–903.

(23) Deschler, F.; Price, M.; Pathak, S.; Klintberg, L. E.; Jarausch, D.-D.; Higler, R.; Huttner, S.; Leijtens, T.; Stranks, S. D.; Snaith, H. J. *The Journal of Physical Chemistry Letters* **2014**, *5*, 1421–1426.

(24) Timpu, F.; Sergeyev, A.; Hendricks, N. R.; Grange, R. *ACS Photonics* **2016**, *4*, 76–84.

(25) Shilkin, D. A.; Shcherbakov, M. R.; Lyubin, E. V.; Katamadze, K. G.; Kudryavtsev, O. S.; Sedov, V. S.; Vlasov, I. I.; Fedyanin, A. A. *ACS Photonics* **2017**, *4*, 1153–1158.

(26) Markovich, D. L.; Ginzburg, P.; Samusev, A.; Belov, P. A.; Zayats, A. V. *Optics Express* **2014**, *22*, 10693–10702.

(27) Phillips, L. J.; Rashed, A. M.; Treharne, R. E.; Kay, J.; Yates, P.; Mitrovic, I. Z.; Weerakkody, A.; Hall, S.; Durose, K. *Data in Brief* **2015**, *5*, 926–928.

(28) Regmi, R.; Berthelot, J.; Winkler, P. M.; Mivelle, M.; Proust, J.; Bedu, F.; Ozerov, I.; Begou, T.; Lumeau, J.; Rigneault, H.; Garca-Paraj, M. F.; Bidault, S.; Wenger, J.; Bonod, N. *Nano Letters* **2016**, *16*, 5143–5151.

(29) Cambiasso, J.; Grinblat, G.; Li, Y.; Rakovich, A.; Cortés, E.; Maier, S. A. *Nano Letters* **2017**, *17*, 1219–1225.

(30) Chew, H. *Physical Review A* **1988**, *38*, 3410.

(31) Diroll, B. T.; Guo, P.; Schaller, R. D. *Nano Letters* **2018**, DOI: 10.1021/acs.nanolett.7b04099.

(32) Makarov, S. V.; Zalogina, A. S.; Tajik, M.; Zuev, D. A.; Rybin, M. V.; Kuchmizhak, A. A.; Juodkazis, S.; Kivshar, Y. *Laser & Photonics Reviews* **2017**, *11*, 1700108.

(33) Fu, Y. H.; Kuznetsov, A. I.; Miroshnichenko, A. E.; Yu, Y. F.; Lukiyanchuk, B. *Nature Communications* **2013**, *4*, 1–6.

(34) Camacho-Morales, R.; Rahmani, M.; Kruk, S.; Wang, L.; Xu, L.; Smirnova, D. A.; Solntsev, A. S.; Miroshnichenko, A.; Tan, H. H.; Karouta, F. *Nano Letters* **2016**, *16*, 7191–7197.

(35) Lewi, T.; Iyer, P. P.; Butakov, N. A.; Mikhailovsky, A. A.; Schuller, J. A. *Nano Letters* **2015**, *15*, 8188–8193.

(36) Noh, J. H.; Im, S. H.; Heo, J. H.; Mandal, T. N.; Seok, S. I. *Nano Letters* **2013**, *13*, 1764–1769.

(37) Sadhanala, A.; Deschler, F.; Thomas, T. H.; Dutton, S. E.; Goedel, K. C.; Hanusch, F. C.; Lai, M. L.; Steiner, U.; Bein, T.; Docampo, P. *The Journal of Physical Chemistry Letters* **2014**, *5*, 2501–2505.

(38) Yoon, S. J.; Draguta, S.; Manser, J. S.; Sharia, O.; Schneider, W. F.; Kuno, M.; Kamat, P. V. *ACS Energy Letters* **2016**, *1*, 290–296.

(39) Hoke, E. T.; Slotcavage, D. J.; Dohner, E. R.; Bowring, A. R.; Karunadasa, H. I.; McGehee, M. D. *Chemical Science* **2015**, *6*, 613–617.

(40) Moss, T. *Proceedings of the Physical Society. Section B* **1950**, *63*, 167.

(41) Makarov, S.; Sinev, I.; Milichko, V.; Komissarenko, F.; Zuev, D.; Ushakova, E.; Mukhin, I.; Yu, Y.; Kuznetsov, A.; Belov, P.; Iorsh, I.; Poddubny, A.; Samusev, A.; Kivshar, Y. *Nano Letters* **2018**, *18*, 535–539.

(42) Lockwood, D. J.; Wu, X.; Baribeau, J.-M.; Mala, S. A.; Wang, X.; Tsybeskov, L. *Frontiers in Materials* **2016**, *3*, 12.

Graphical TOC Entry